Technical Report No. 32-520

Arc Discharge in a Parallel Flow of Argon

Hiroshi Sato

JPL-TR-32-520

jpl

JET PROPULSION LABORATORY
CALIFORNIA INSTITUTE OF TECHNOLOGY
PASADENA, CALIFORNIA

October 31, 1963   23p

Arc Discharge in a Parallel Flow of Argon

Hiroshi Sato

John Laufer, Chief
Fluid Physics

CONTENTS

TABLES

FIGURES

ABSTRACT

12 947

A dc arc discharge was made in a parallel subsonic flow of argon with a discharge current of about 70 amp and a flow velocity as large as 27 meter/sec at a pressure of 300 Torr and as large as 70 meter/sec at 100 Torr. The flow stabilizes the arc, and when the discharge current is kept constant, the observed diameter of the arc decreases and the voltage drop across electrodes increases as the flow speed is increased. Detailed experimental results indicate that the electric field intensity in the positive column increases almost linearly with the flow speed. A spectroscopic measurement shows a temperature rise near the arc axis as an effect of the flow. Measurements of the time-mean velocity as well as the fluctuation were made by use of a hot-wire anemometer. Physical properties of an argon plasma were calculated assuming thermal equilibrium. The heat balance of a long cylindrical plasma with radial gas flow was treated theoretically. The solution of the energy equation shows a fair agreement with the experimental results for the field intensity and temperature distributions.

AUTHOR

I. INTRODUCTION

The positive column of a high-pressure arc is in thermal equilibrium owing to frequent collisions among the particles and is electrically neutral as a whole. It is known that in the positive column of a high-current arc the maximum temperature is on the order of 10^4 °K, and the ionization fraction is around $10^{-2} \sim 10^{-1}$. A free-burning arc is, on the other hand, usually unstable owing to the convective flow around the arc. A great many papers concerning studies of arc positive columns have been published. Arcs can be stabilized by a revolving flow around the arc. The electric field and temperature distribution have been measured in the stabilized arc. However, in order to create a high-temperature, contamination-free plasma jet, the behavior of an arc in a

subsonic and a supersonic flow must be clarified. Recently, two experimental investigations have been made on an arc in a flow. An experiment with the flow normal to the arc was made by P. G. Thiene et al (Ref. 1). They found that the arc is blown off at a relatively low wind speed, on the order of 1 meter/sec. They calculated the "stiffness" of the arc in the normal flow by using a simple theoretical model and showed a fair agreement between the theory and experiment. An arc discharge in a Poiseuille flow was investigated by H. Emmons and others (Ref. 2). The wall pressure and electric field were measured and experimental results were explained by a simplified theory.

In the present investigation the flow is uniform and parallel to the arc. If the flow speed is high enough compared with the upward free convection velocity, the arc might be stabilized. On the other hand, the increase of the heat convection due to the radial velocity component decreases the temperature of the arc at the outer region. If the discharge current is kept constant, the current density at the inner region should increase and this might result in an increase of temperature. The main purpose of the present investigation is to clarify these points experimentally and theoretically.

One shortcoming of the parallel configuration is the fact that we cannot eliminate the effect of the upstream electrode on the flow. In other words, the arc burns in the wake of the upstream electrode. The velocity gradient and turbulence in the wake might have influences on the nature of the arc. However, the wake of an axisymmetric body is not too complicated, and it is possible to investigate the details of the wake by conventional aerodynamic means when the arc is not present.

Measurements were made on the electric field and temperature distribution in the positive column. The physical properties of argon plasma were calculated, and the energy equation was solved with the radial component of flow being taken into account. Experimental and theoretical results were compared.

II. EXPERIMENTAL ARRANGEMENT

The experiments were carried out in one of the low-density tunnels at the Jet Propulsion Laboratory. Figure 1 shows the experimental arrangement. Argon was supplied from a bank of high-pressure bottles through a pressure regulator to a settling chamber. Argon was chosen as the working gas because it is free from dissociation, and the physical properties of argon are well known. The gas is accelerated by a converging nozzle carefully designed from an aerodynamical viewpoint in order to produce a uniform and parallel flow and to minimize the turbulence at the test-section. The diameters of the settling chamber and nozzle exit are 20 and 5 cm, respectively. A damping screen installed in the settling chamber in conjunction with the large contraction ratio serves to reduce the turbulence. The flow from the nozzle is issued into a large tank. Since there is no solid wall around the flow,

optical observations and probe measurements are made easily. On the other hand, the mixing at the flow boundary restricts the available length of a uniform flow region to about 6 cm from the nozzle. Argon in the tank is pumped out by large mechanical pumps. The range of static pressure and mass flow are determined by the pumping capability. The maximum possible speed at the test-section is 27 meter/sec at a pressure of 300 Torr (mm Hg) and 72 meter/sec at 100 Torr.

The upstream electrode is suspended on the centerline of the nozzle by means of three fine spokes at each of two stations in the settling chamber. By this arrangement the turbulence generated by the supports is minimized and the axial symmetry of the flow is maintained. The ratio of cross-sectional area of the electrode to that of the
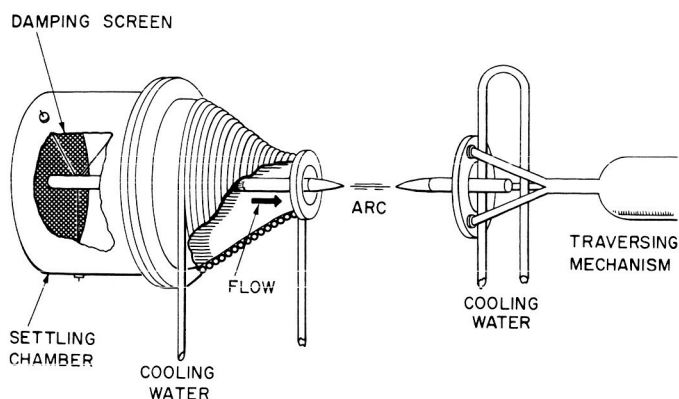
Fig. 1. Experimental arrangement

exit nozzle is about 1:25. Therefore, the blockage effect of the electrode is not substantial. The downstream electrode is supported by an insulated ring which in turn is mounted on a traversing mechanism. The positioning of the traversing mechanism is accomplished from outside of the tunnel with an accuracy of 0.1 mm in three directions.

The flow velocity at the test-section is determined by a pitot tube and manometer. Distributions of the time-mean and fluctuating velocities behind the upstream electrode are measured by a hot-wire anemometer and a compensated amplifier. Electrode tips, both anode and cathode, are made of thoriated tungsten, the diameter being 0.95 cm. They were machined and ground in an

aerodynamically smooth shape in order to keep the boundary layer on the electrode laminar and to prevent a separation of the boundary layer. The tips are attached to brass tubes of exactly the same diameter in which cooling water circulates. Thermocouples are inserted at the entrance and exit of the cooling water tubing in order to allow observation of the temperature rise of the water. The erosion of electrode material is very small. Electrodes are changed after about 10 running hours.

The power supply for the discharge is an arc welder. It delivers a dc current up to 150 amp at 100 volts. Since the required discharge voltage is only about 20 volts, a series resistor is used to give a proper voltage drop. The voltage of power supply is kept as high as possible. By this connection the discharge current is stabilized against changes in the discharge voltage. The ripple voltage of the power supply is around 0.5 volt rms at 70 amperes current.

In order to start an arc the tip of the downstream electrode is brought into contact with the upstream electrode; after the arc is started the downstream electrode is carried back to a desired position. This method is simple and reliable.

The temperature of the arc was determined by an optical method which is based on the measurement of the relative intensity of a spectral line. A grating spectrograph was used with a photomultiplier. Details are to be described later.

III. EXPERIMENTAL RESULTS

A. General Aspects

The discharge current of an axially symmetric arc is expressed by

$$I = \int_0^\infty j \cdot 2\pi r dr = 2\pi \int_0^\infty E\,\sigma\,r dr \qquad (1)$$

where E and σ are the electric field intensity in the direction of discharge and the local electrical conductivity, respectively. If the arc is long enough, the electric field in the positive column is considered to be uniform and parallel to the axis. Introducing mean values for the conductivity and arc radius (1) reduces to

$$I = \pi\sigma_m r_m{}^2 E \qquad (2)$$

The Joule heating per unit length of positive column is

$$IE = \pi\sigma_m r_{m^2} E^2 \qquad (3)$$

The heat transfer from the arc to the surrounding gas is enhanced by the flow. If the discharge current is kept constant, the electric field E must increase in order to balance the increased heat transfer. Considering Eq. (2), this increase of E results from the decrease of the product $\sigma_m r_m^2$.

The radius of the arc is observed in such pictures as shown in Fig. 2. The "optical radius" definitely decreases as the flow speed is increased. This tendency is generally true for cases of different pressures and polarities. Although the "electrical radius" r_m in Eqs. (2) and (3) is different from the optical radius, it is probable that the arc shrinks and that the mean conductivity increases as the flow speed is increased. The increase of conductivity indicates an increase of temperature because, in the range of the present experiment, the conductivity is a monotonically increasing function of temperature.

Another noticeable effect of the flow is the stabilization of the discharge. Without flow the arc bends upward as shown in Fig. 2a. The flow makes the arc straight and axially symmetric. The upward bend is due to the natural convection around the arc. An arc in free space moves up and down and sometimes turns around the axis. This instability is eliminated by the axial flow when the speed is high enough compared with the free convection speed.

The current-voltage relation of the discharge is shown in Fig. 3. The voltage drop increases as the flow speed is increased, although the general trend of $V \sim I$ curves remains unchanged. An increase of voltage drop does not necessarily indicate an increase of the electric field intensity in the positive column because the cathode and anode drops may also be influenced by the flow. A measurement of the electric field in the positive column was made, and the results are described in Section IV.

As shown in Fig. 4, the power input to the arc increases almost linearly as the flow speed is increased. The
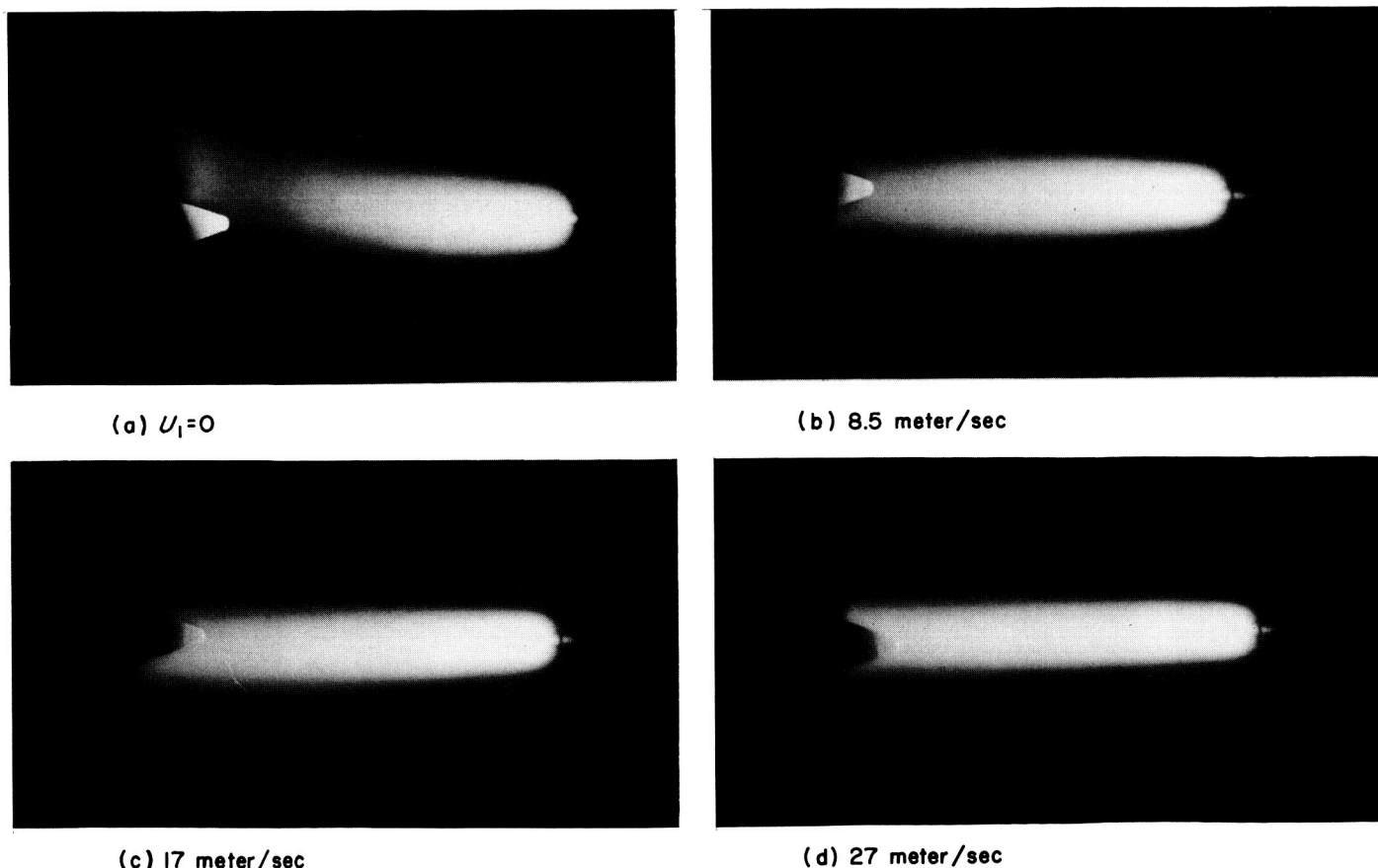

(a) $U_1 = 0$

(b) 8.5 meter/sec

(c) 17 meter/sec

(d) 27 meter/sec

Fig. 2. Arc at various free-stream velocities
Flow from right to left. Pressure, 300 Torr; upstream cathode;
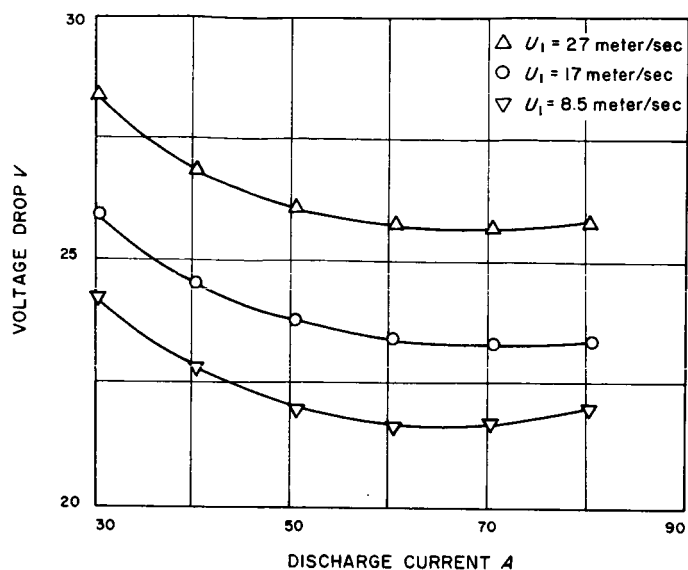electrode gap, 5 cm; discharge current, 70 amp

Fig. 3. Voltage drop across electrodes
Pressure, 300 Torr; upstream cathode; electrode gap, 5 cm

electric power is converted to heat. Since the radiation from the arc is small, the excess power due to the flow is partly carried away by the flow and partly given to the electrodes. The power distribution was measured by recording the temperature rise of the cooling water for the two electrodes and nozzle wall. The rest of the power is supposed to be carried away by the gas. Results at $p = 300$ Torr are shown in Fig. 5 for both cases of polarity. When there is no flow, half of the total power input is consumed at the anode. In the presence of flow, the heat transfer to the downstream electrode increases. When the anode is placed upstream, the downstream edge of the converging nozzle is heated by the natural
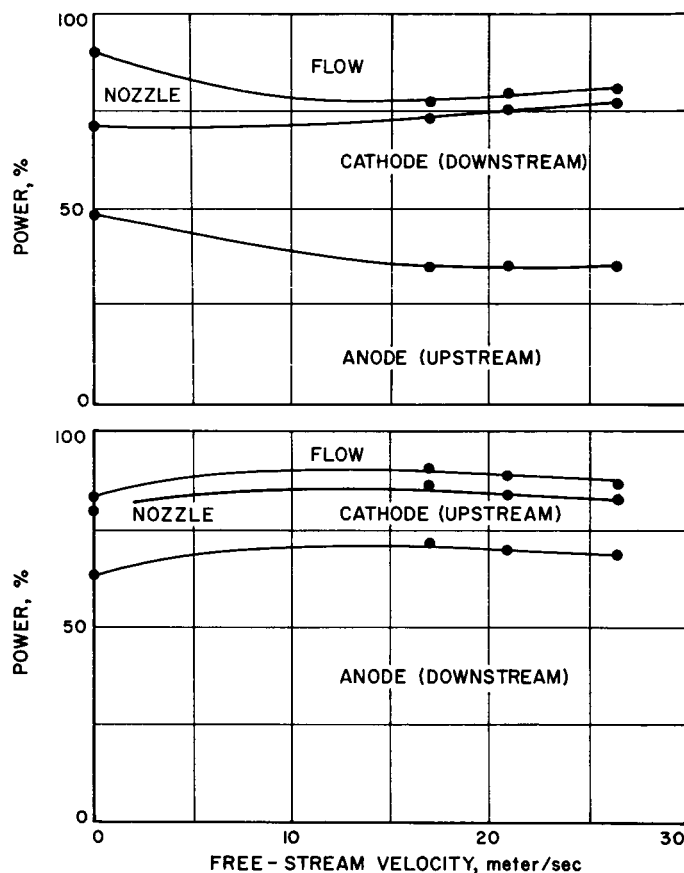

Fig. 4. Power dissipation
Pressure, 300 Torr; upstream cathode; electrode gap, 5 cm

Fig. 5. Power distribution
Pressure, 300 Torr; electrode gap, 5 cm; discharge current, 70 amp

convection around the anode. This explains the difference of power distribution for different polarity. The power given to the flow does not exceed 20%. A more detailed discussion of the results of the present experiment will not be made, because the power distribution depends heavily on the configuration of the electrodes and nozzle and also on the arrangement for cooling.

B. Flow Field

With the configuration of flow and discharge as shown in Fig. 1, the arc burns in the wake of the upstream electrode. The flow field behind the electrode needs to be understood in order to allow a meaningful discussion of the effect of the flow. Since no precise flow measurement seems to be possible when the arc burns, the flow field surveys were made without an arc. The downstream electrode was taken out for the convenience of traversing an anemometer. Air was used as the working gas for purposes of economy. Since the kinematic viscosities of air and argon at a pressure of 300 Torr and temperature of 20°C are 0.39 and 0.34 cm²/sec, respectively, the flow
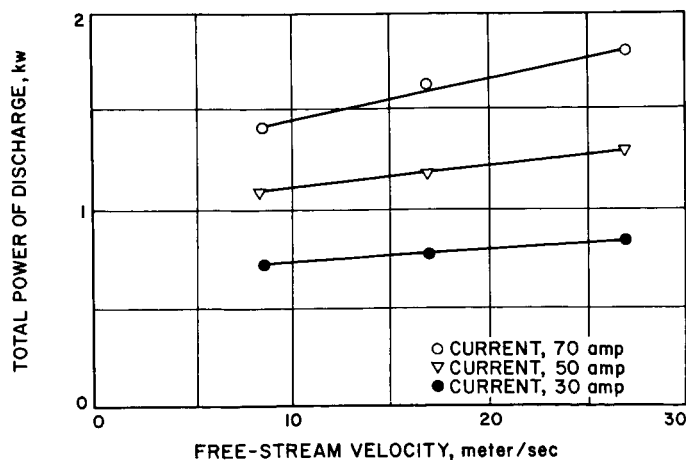
pattern of air and argon with the same free-stream velocity should be almost identical.

Measurements of the mean-velocity distribution and velocity fluctuation were made by means of a hot-wire anemometer and conventional electronic equipment, including a compensating amplifier, power amplifier, squaring output meter, etc. Measurements were made only of the streamwise velocity component.

Figure 6 shows an example of the measured mean-velocity and fluctuation distributions at $p = 300$ Torr and free-stream velocity $U_1 = 17$ meter/sec. By the mean-velocity measurement, it was confirmed that the wake is axially symmetric.

Since the tip of the electrode is sharp there might be no direct relationship between the diameter of the upstream electrode and the radius of the wake. The mean-velocity distribution at $X = 2$ mm shows a small dead-water region. The wake develops downstream, and the velocity defect at the usual position of the downstream electrode tip ($X = 50$ mm) is about 15% of the free-stream velocity. A mixing zone develops from the edge of the nozzle. The mean-velocity distribution shows that the uniform flow region extends from a radius of 10 mm to about 16 mm at $X = 50$ mm. On the other

Fig. 7. Waveform of u-fluctuation detected by hot-wire anemometer

hand, the distribution of velocity fluctuation shows that the mixing zone extends further inside and that, at $X = 50$ mm, the region of velocity fluctuation in the wake almost joins with that of the mixing zone. In order to avoid the disturbing effect of the mixing zone, the electrode spacing must be kept less than 50 mm. The root-mean-square of the u'-fluctuation grows downstream, reaches 15% of free-stream velocity at $X = 20$ mm, and gradually decreases downstream. The positions of the peaks in the radial distribution roughly coincide with the positions of maximum shear in the mean-velocity distribution.

The waveform of the u'-fluctuation was recorded photographically from the synchroscope screen and is shown in Fig. 7. A regular sinusoidal waveform is observed at small X when the flow speed is low. The frequency of the fluctuation is around 150 to 600 cps for free-stream velocity from
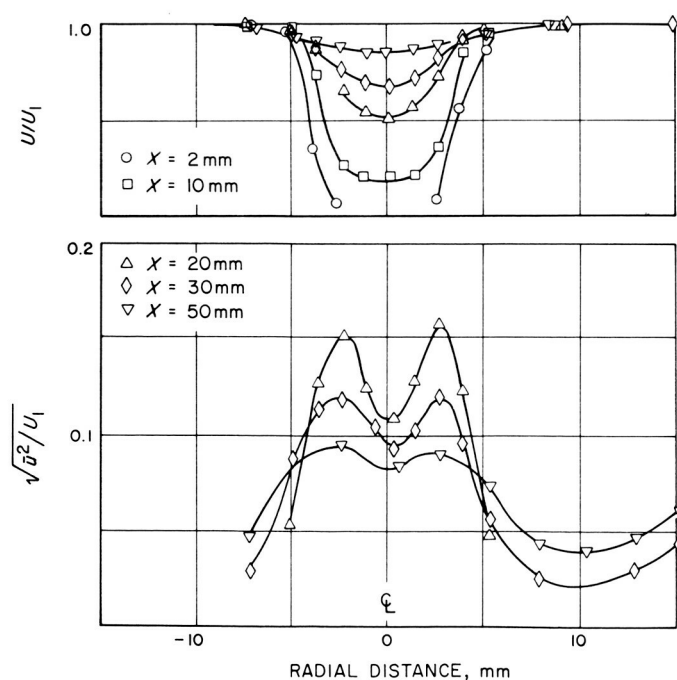

Fig. 6. Time-mean-velocity distribution and turbulence intensity at various stations behind upstream electrode

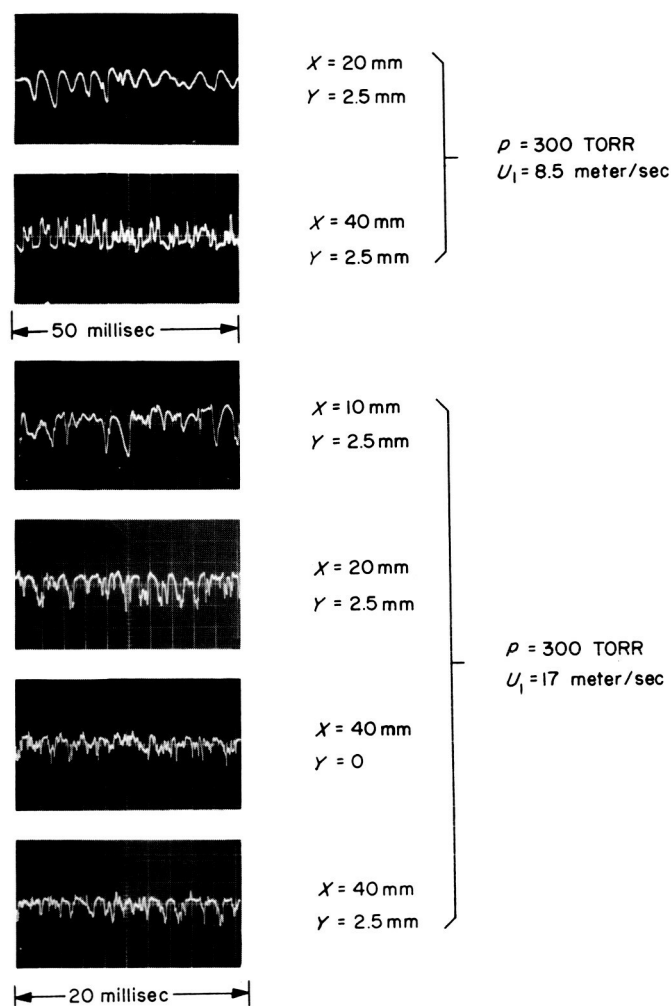Pressure, 300 Torr; free-stream velocity, 17 meter/sec

8 to 25 meter/sec and the Strouhal number defined as fd/U_1 (where f is the frequency, d is the diameter of the up-stream electrode, and U_1 is the free-stream velocity) increases from 0.15 to 0.3 as U_1 is increased. Considering that the diameter of the electrode is not of primary importance for the wake of a sharp-tail body, this variation of Strouhal number is not unreasonable. Fluctuations of periodic waveform did not seem to be present at a high-free-stream velocity. Generally, a sinusoidal fluctuation is expected when a small disturbance given to the wake is amplified linearly. The sinusoidal velocity fluctuation in a two-dimensional wake was investigated in detail (Ref. 3). A distortion of waveform takes place when a nonlinear effect appears in the process of development of velocity fluctuation. Detailed measurements are needed in order to learn more about the sinusoidal fluctuation.

At large X, the waveform is very irregular and the wake is definitely turbulent regardless of the flow speed. The velocity distribution of a turbulent axisymmetric wake is expressed very well by an empirical formula

$$\frac{U}{U_1} = 1 - \frac{k}{(x - x_0)} \exp\left(- ay^2\right) \qquad (4)$$

in which $a = 0.693$, and k and x_0 are determined by a proper curve fitting. Coordinates x and y are X/b and Y/b, respectively and b is the radius at which the velocity defect becomes one-half of the defect on the axis. At $U_1 = 17$ meter/sec, $p = 300$ Torr, k and x_0 are found to be 2.5 and 1.7, respectively, and b is 0.3 cm. The radial velocity component V as computed from the continuity equation is

$$\frac{V}{U_1} = - \frac{k}{(x - x_0)^2 y} \frac{1}{2a}\left[\exp\left(-ay^2\right) - 1 \right] \qquad (5)$$

Experimental and calculated distributions of U and V are shown in Fig. 8. Since no direct measurement of the radial velocity V was made, there are no experimental points on the curves at the bottom. The distribution of V is to be used for computing the convective heat flow.

C. Electric Field

The electric field intensity in a positive column was determined from measurements of the voltage across the electrodes. Since the total voltage is the sum of the voltage drops of the cathode and anode regions and the positive column, it is necessary to determine their values
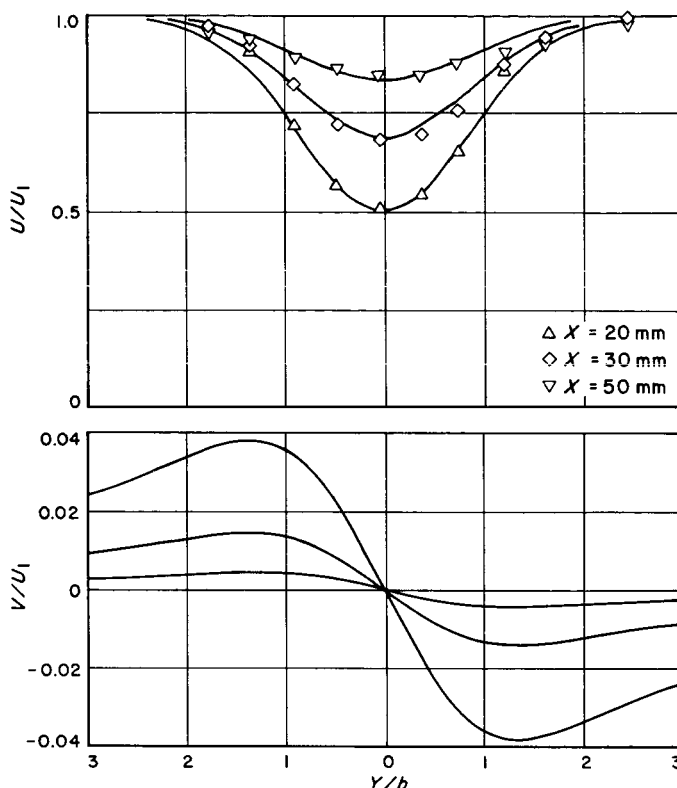

Fig. 8. Approximate velocity distribution
Pressure, 300 Torr; free-stream velocity, 17 meter/sec

separately. When the arc is long enough and the pressure is not too low, it is expected that the structure of the electrode region might not be influenced by a change in the length of the arc. The electric field intensity in the positive column can be determined by changing the electrode gap, keeping the discharge current constant. The voltage between electrodes, measured at various positions of the downstream electrode along the flow direction, is shown in Fig. 9. Zeros of the voltage scale are shifted in order to avoid confusion. The lines are slightly curved when the gap is small, but are almost straight for a large gap. This fact tends to confirm the foregoing speculation. The gradient of the straight portion gives the field intensity. Other experimental results obtained for the opposite polarity at 300 Torr and for both polarities at 100 Torr are similar in general trend; i.e., for a gap larger than about 3 cm, the relation of voltage drop and gap length is linear. The field intensity determined as explained above is shown in Fig. 10. The intensity is less for a lower pressure. For both pressure levels, the field intensity is less when the upstream electrode is negative (cathode). The intensity changes nearly linearly with the flow speed. More detailed discussion of these facts will be presented in the following sections.
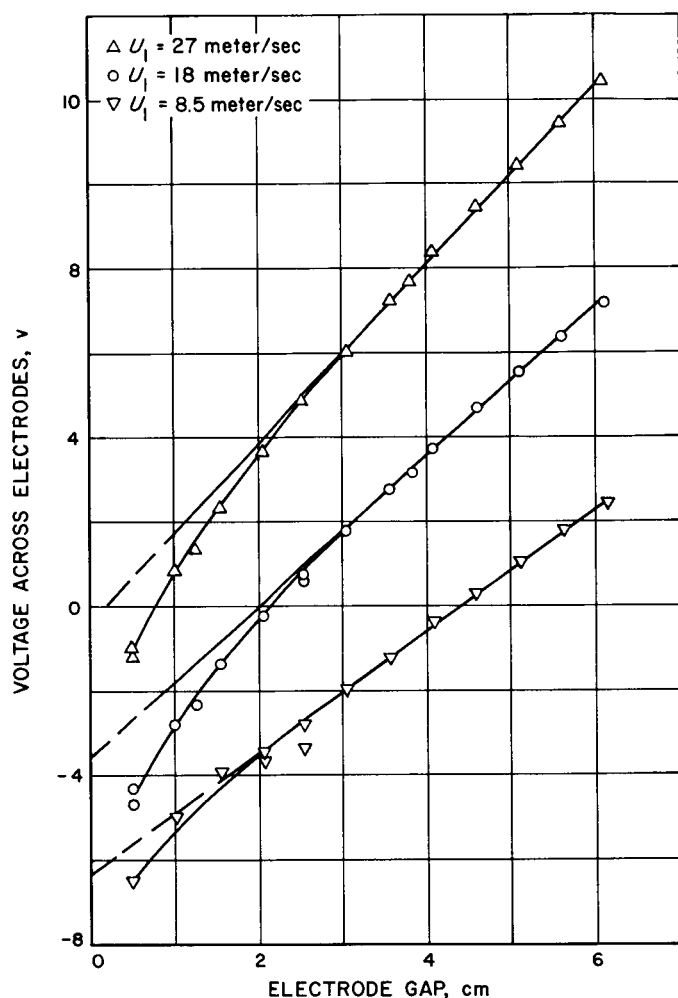
Fig. 9. Voltage drop vs electrode gap
Pressure, 300 Torr; upstream cathode; discharge current, 70 amp;
zero volt for $U_1 = 8.5$ meter/sec, 23.4 volt

Fig. 10. Electric field intensity in positive column

The field intensity at $U_1 = 0$ was not measured with good accuracy because the discharge was usually unstable without flow. Even when the discharge is stable enough, the measured result does not correspond to the case of $U_1 = 0$ because there is a free convection around the arc. The field intensity which should exist without convection is obtained by an extrapolation of the data with flow as shown by broken lines in Fig. 10. Extrapolations for the opposite polarity converge to the same values, 1.1 volt/cm and 0.85 volt/cm for pressures 300 Torr and 100 Torr, respectively.

The extrapolation of the straight portion of the voltage-gap curve gives a sum of cathode and anode drops. This value is a fictitious electrode fall because in this reasoning it is assumed that the thickness of the fall region is zero and that the uniform plasma extends from cathode
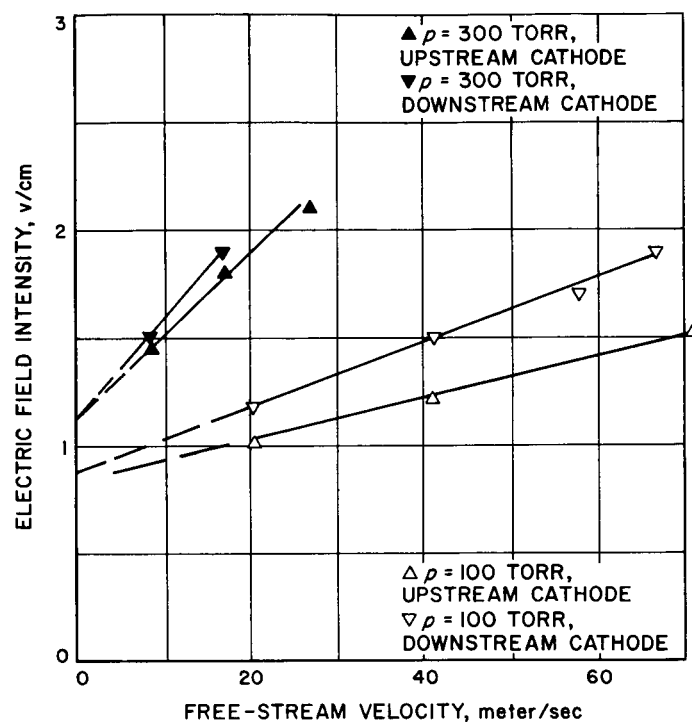
to anode. Results shown in Fig. 11 demonstrate that the drop is larger for the lower gas pressure and that the dependence on flow velocity is small.

D. Temperature Distribution

The plasma temperature was obtained from measurements of the spatially resolved relative spectral line intensity. This method was originally developed by Larenz (Ref. 4) and used successfully for an argon arc by Olsen (Ref. 5). The intensity of the line spectrum is proportional to the number density of light-emitting particles, which in turn is proportional to the product of the number density of total atoms (or ions) and exp $(-E_m/kT)$, E_m being the energy level of the higher state in the transition. The number densities of atoms and ions in an equilibrium plasma can be calculated by use of the Saha equation. Owing to the ionization, the number density of atoms decreases as the temperature of the gas increases. On the other hand, the exponential factor exp $(-E_m/kT)$ increases with the temperature. These two effects give a maximum in the number density of light-emitting atoms at a certain temperature. For argon at 300 Torr and 100 Torr, the relative intensity of $\lambda 4300$ as a function of temperature has been calculated and is shown in Fig. 12. The procedure of calculation was the same as that of Olsen (Ref. 5). There are maxima at 13,700°K for pres-
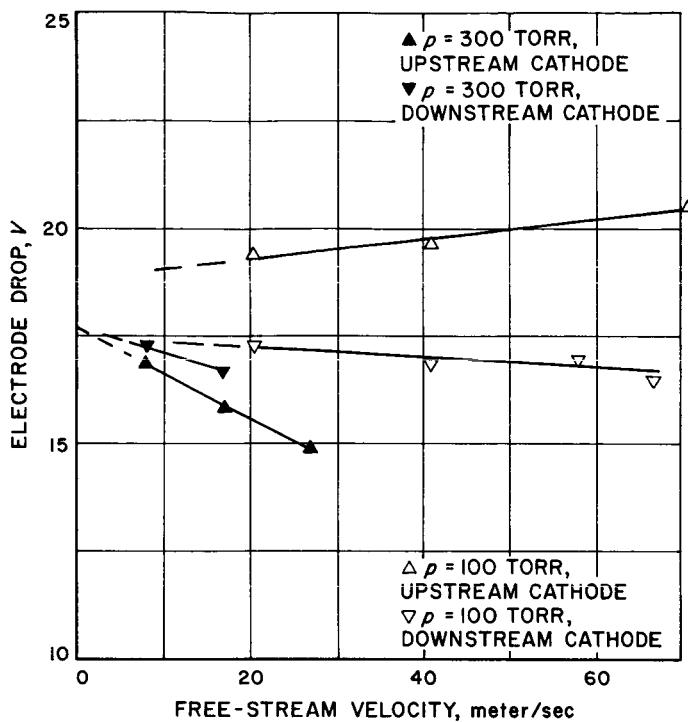
Fig. 11. Electrode drop (sum of anode and cathode drops)

sure 100 Torr and 14,500°K for 300 Torr, respectively. Since the temperature of argon in the present experiment does not exceed 18,000°K, it was not necessary to consider ionic lines. The lowest measurable temperature is restricted by the capability of detecting weak light. By consideration of stray light in the optical system and noise from the phototube, the limit is estimated to be about 8,000°K, at which the light intensity is less than
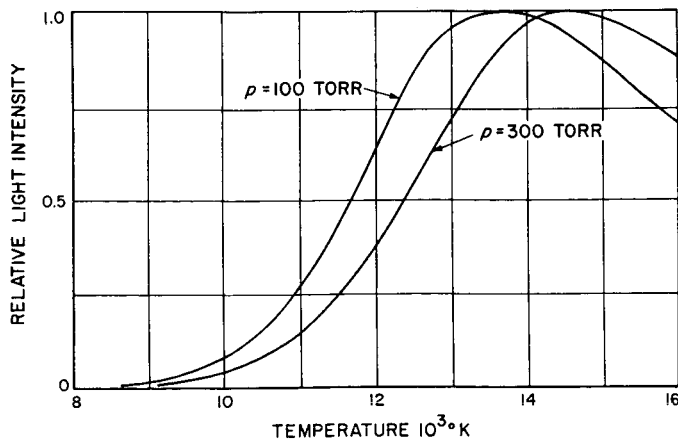

Fig. 12. Calculated relative light intensity emitted from argon plasma

0.1% of maximum value. More detailed descriptions of the procedure are given in Refs. 4 and 5.

The optical system consists of a projecting system, spectrograph, magnifying system, and photomultiplier. In the projecting system, a 40-cm-diameter concave mirror of 3.6-meter focal length and several small plane mirrors were used. By rotating the plane mirrors with micrometer screws, it is possible to shift the image in the X-direction (the direction of discharge) and Z-direction (normal to the discharge). By a proper arrangement of the mirrors the light beam becomes exactly perpendicular to the plane of the entrance slit of the spectrograph. An Ebert-type plane-grating spectrograph was used. It has a dispersion of 33 Å/mm for the first order. Second-order spectra were used in the present experiment in order to increase the dispersion. First-order lines of double wavelength have no disturbing effect since they are not intense and the photomultiplier used has no sensitivity in the infrared region. The width of the entrance slit is about 50 microns. The magnifying system is attached to the exit of the spectrograph. The image of the spectrum is projected on a plate with a 0.5-mm-diameter pinhole. An RCA 931-A photomultiplier is used to detect the intensity of light passing through the hole. A branch of the magnifying system makes it possible to photograph the spectrum simply by turning a plane mirror. This arrangement was found useful for checking the performance of the whole optical system. Since the magnification is about 6, the dispersion obtained at the pinhole plate is about 2.7 Å/mm for the second-order spectrum. Since the image of the arc is shifted by plane mirrors in the projecting system, there are no mechanical or optical problems in obtaining a distribution of intensity in X- and Z-directions.

The atomic line $\lambda 4300$ was selected for intensity measurements because it is sufficiently intense and free from disturbing adjacent lines. The contribution of the background continuous spectrum was subtracted properly.

The observed intensity distribution is an integrated value of the existing radial distribution. Neglecting the self-absorption, a true distribution $i(r)$ of an axially symmetric source can be calculated from the observed distribution $I(Z)$ by the well-known Abel equation

$$I(Z) = 2 \int_r^\infty \frac{i(r)r\,dr}{\sqrt{r^2 - Z^2}} \qquad (6)$$

A numerical solution of this equation for $i(r)$ was obtained by Pearce (Ref. 6). The actual calculation was

carried out using 12 radial divisions by means of Pearce's table. A calculated result with an increased number of divisions gave no significant difference in the final result. For instance, 20% error in the relative line intensity gives an error of 100°C at 10,000°K. Considering that so many assumptions and simplifications are made in the procedure of determining temperature from line intensity, we might expect a larger error than 100°C in obtaining absolute temperature. Therefore, it seemed to be of no benefit to use more than 12 divisions.

Figure 13 shows an example of the spectrum in the violet region. The line used for intensity measurement is indicated by an arrow. Impurity lines are not observed in the positive column region. Spectra of tungsten and other substances were observed in regions near the electrodes. The coordinate normal to the wavelength scale corresponds to the direction normal to the arc. Figure 14 shows the radial temperature distributions at various X-stations. In this case, the tips of the anode and cathode correspond to $X/D = 0$ and $X/D = 1.0$, respectively. The temperature near the cathode exceeds 17,000°K. In the region between $X/D = 0.30$ and 0.70 the temperature distribution is almost independent of X/D. This indicates that there is a uniform plasma in the middle of the arc. Figure 15 shows the radial distribution of temperature at the center $(X/D = 0.5)$ of the arc for

Fig. 14. Temperature distribution

Pressure, 300 Torr; downstream cathode; electrode gap, 5 cm; free-stream velocity, 17 meter/sec; discharge current, 70 amp
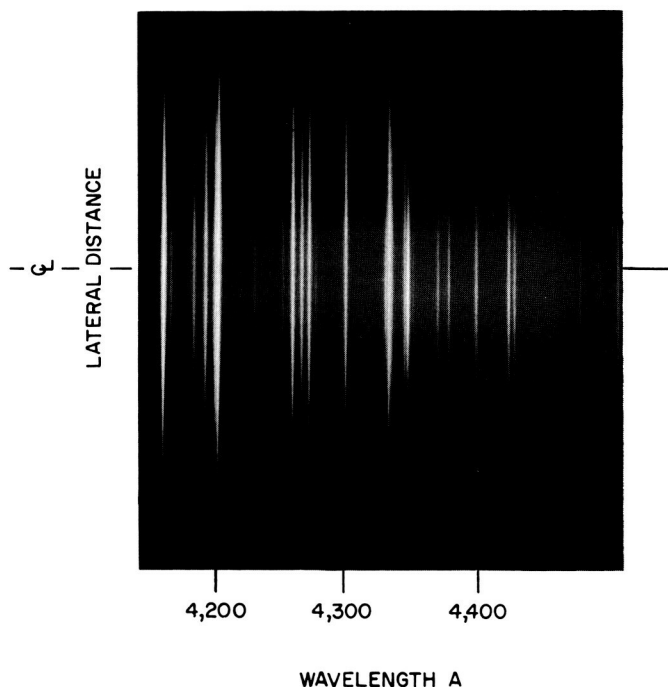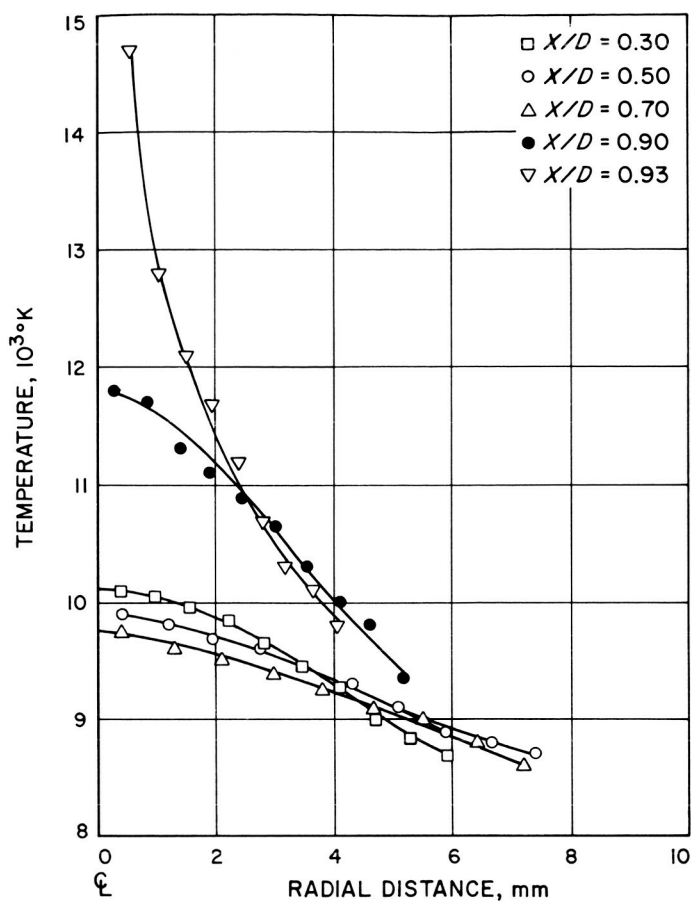

Fig. 13. Violet region spectrum of argon arc
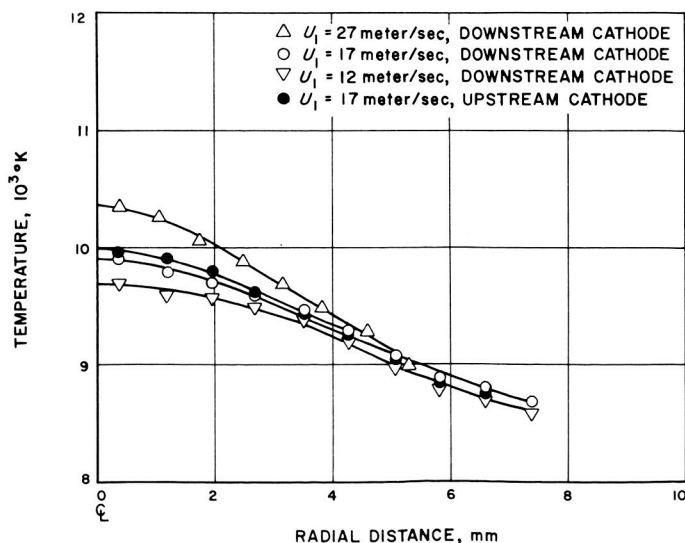
Pressure, 100 Torr; no flow

Fig. 15. Temperature distribution at $X/D = 0.5$

Pressure, 300 Torr; electrode gap, 5 cm; discharge current, 70 amp

various flow velocities. It is seen that for higher flow speed the temperature near the axis is higher. The temperature distributions are about the same for both polarities of the arc. The temperature on the center line at $X/D = 0.5$ is plotted against flow velocity in Fig. 16. The temperature increases linearly with flow velocity.

E. Fluctuations

It has been observed that the flow stabilizes the arc. When there is no flow around the arc, the cathode and/or anode spots move around the electrode tips, and at the same time the visual shape of the arc changes. The flow around the arc inhibits this kind of instability. The stabilization effect is clearly noticed by observing the voltage across the electrodes. Without flow, a sudden change of voltage takes place within a time interval of the order of seconds or minutes. The sudden jump and pulsive disturbance do not occur when a flow exists. On the other hand, there is a velocity fluctuation in the flow which causes another kind of voltage fluctuation with higher frequency. It is well known that the voltage fluctuation of an arc discharge is caused by various kinds of electrical oscillation. Since, at present, we are interested in the voltage fluctuation due to the velocity fluctuation in the flow, an attempt was made to eliminate unnecessary fluctuations. The hot-wire measurement indicates that the frequency range of velocity fluctuation extends roughly from 100 to 2000 cps. Therefore, a band-pass filter having a frequency range from 150 to 2000 cps was used in order to exclude high-frequency voltage fluctuations which might be caused by electrical oscillations.
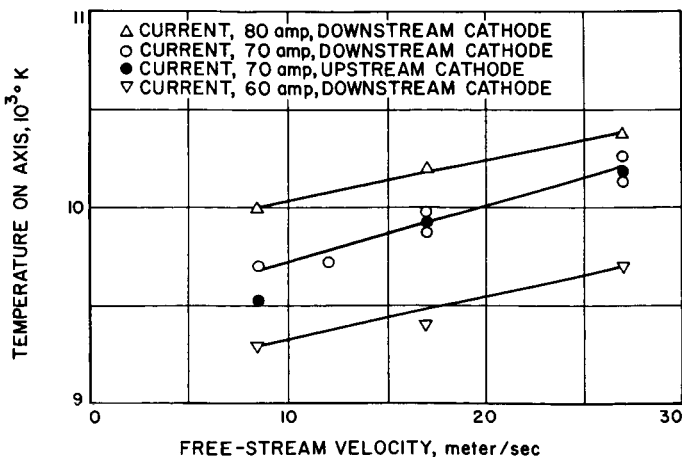

Fig. 16. Temperature on axis at X/D = 0.5

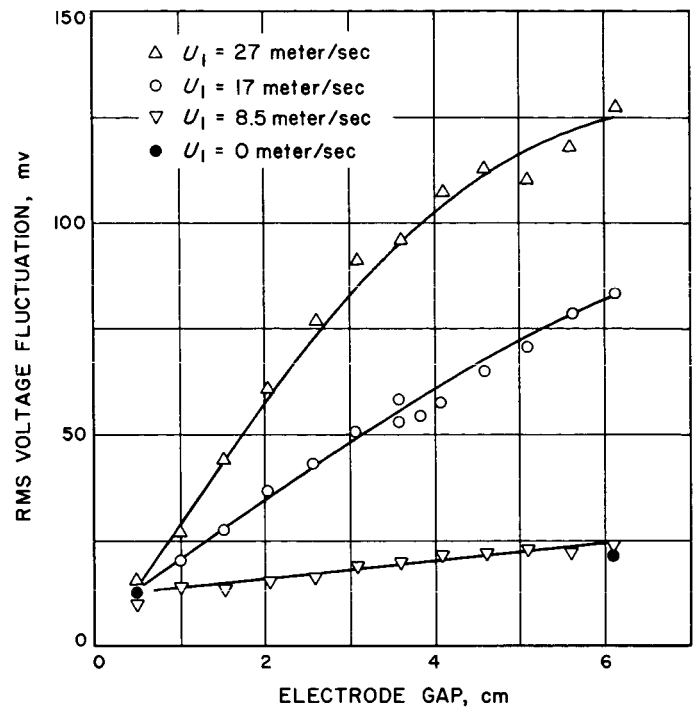Pressure, 300 Torr; electrode gap, 5 cm

Fig. 17. Voltage fluctuation

Pressure, 300 Torr; upstream cathode; discharge current, 70 amp; frequency range, 150 ∼ 2,000 cps

The observed waveform of the voltage fluctuation showed no dependence upon the wind speed. Measured rms values of voltage fluctuation are shown in Fig. 17. The relationship between voltage fluctuation and electrode gap is almost linear. This fact suggests that there are two kinds of fluctuations, one being contributed by the cathode and anode regions, and the other by the positive column. However, the extrapolation of the curves to zero gap-width indicates that the contribution of the electrode regions is small when the flow velocity is high. In addition, there are some other reasons for believing that the contribution is small. First, the velocity fluctuation near electrodes might be small compared with that in the free space between them. The variation of static-electrode fall with respect to the flow velocity was shown in Fig. 11. The variation of static voltage across the positive column with respect to the flow velocity is obtained from Fig. 10 assuming the length is 5 cm. At $p = 300$ Torr these two voltage drops are about $- 0.1$ and 0.2 volt per 1 meter/sec flow charge, respectively. Therefore, the voltage fluctuation due to the velocity fluctuation is small near the electrode. Second, the large heat capacity of the electrodes tends to inhibit the temperature fluctuations that cause voltage fluctuations.

Table 1. Voltage fluctuation (pressure, 300 Torr)

U_1, meter/sec	8.5	17	27
ED, v	7	9	10.5
$\sqrt{\overline{e^{-2}}}/$ ED, %	0.3	0.8	1.1

The voltage fluctuation as a fraction of voltage drop of the positive column has been calculated under the assumption that the voltage fluctuation originates only within the positive column and is shown in Table 1. The fraction is almost proportional to the free-stream velocity. This result seems reasonable, because the amplitude of the velocity fluctuation is usually proportional to the free-stream velocity, and the voltage fluctuation is caused by the velocity fluctuation. The velocity fluctuation is about 10% of the mean value, while the voltage fluctuation is 1% or less. The disparity can be attributed to the fact that the voltage fluctuation across the electrodes is an integrated value of the local fluctuation. The contribution of the velocity fluctuations of high frequency—in other words, of short wavelength—might be very small.

For the case $U_1 = 17$ meter/sec and $D = 5$ cm, the "cut-off" frequency was found to be about 340 cps. Therefore, roughly speaking, a velocity fluctuation of frequency less than 340 cps contributes to the voltage fluctuation. Voltage fluctuations of frequency higher than 340 cps probably originate from sources other than velocity fluctuations.

The detection of luminosity fluctuations was also attempted. For the case of the same spectral line as was used for the temperature measurement, the fluctuation of intensity is directly related to the temperature fluctuation in the arc. The noise from a phototube and the fluctuation inherent in the discharge itself make the measurement difficult. Moreover, the measured intensity is the integrated value along the direction of observation. A complete discussion is not possible owing to these difficulties. However, the rms fluctuation as a fraction of the total intensity seems to decrease as the flow velocity increases. For example, the fluctuation level varies from 3 to 1% of the total intensity as U_1 is increased from 8.5 to 27 meter/sec at $p = 300$ Torr, at $X/D = 0.5$, and $D = 5$ cm.

IV. DISCUSSION

The effect of a flow on an arc plasma is twofold. First, ions and electrons moving along the electric field might be retarded or accelerated by the flow. Second, the flow enhances the heat loss from the arc in the form of forced convection. The first process is expected to produce a substantial effect when the speed of flow is comparable to that of the ions and/or electrons. A simple calculation indicates that in the present experiment the drift velocity of ions is comparable to or less than the flow velocity, whereas the drift velocity of the electrons is more than ten times the flow velocity. Since most of the properties of the plasma are determined by the motion of the elec-

trons, the retardation or acceleration of ions might have no substantial effect. The flow speed is not so high that we expect blowoff of the arc or shockwave-like phenomena in the plasma. On the other hand, the convection effect on the heat balance might be large. Here, we have to consider two regions in the arc, one being the region near the electrodes and the other being the positive column. The experimental results so far obtained show a small difference in temperature and electric field when the polarity of discharge is reversed. From the hydro-dynamical viewpoint, the leading and trailing tips of the electrodes are stagnation points. These facts imply a

small effect of the flow on the electrode region. The effect of the flow on the heat balance in the positive column will be discussed in detail.

A. Physical Properties

In order to make a theoretical calculation of the heat balance in an arc, the physical properties of the argon plasma such as electrical conductivity, thermal conductivity, and enthalpy must be known as functions of temperature. Since there are no direct experimental measurements, the electrical conductivity, etc., must be calculated by proper methods.

First, the collision cross section is calculated. For electrons, the total cross-section Q_e is expressed by

$$Q_e = \sum_{i=0} n_i Q_{ei} \tag{7}$$

in which the subscript i denotes the ith-fold ionized particles. For $i = 0$, that is, for the electron–atom collision, the cross section is assumed to be πa^2, where a is the gas kinetic atomic radius. At low temperatures the electrons collide mostly with atoms, while at high temperatures the number density of atoms decreases and collisions with ions become frequent. The electron–ion collision cross section of a partially ionized gas is calculated from the results obtained for a fully ionized gas using the same procedure given by Olsen (Ref. 5). Assuming the electric current to be carried only by electrons, the electrical conductivity σ is expressed as

$$\sigma = e^2 n_e / Q_e \, (3mkT)^{1/2} \tag{8}$$

in which m is the mass of the electron, k the Bolzmann's constant, and e the electronic charge. Equation (8) is compared with the calculated value of conductivity of a fully ionized gas by Spitzer and Härm (Ref. 7). By denoting $\sum_{i=1} n_i Q_{ei} = \overline{Q}_{ei} \, n_+$, $n_+ = \sum_{i=1} n_i$, $\overline{Q}_{ei}$ is given by

$$\overline{Q}_{ei} = 0.567 \, Z_e^4 \log q \cdot n_e / \gamma_E \, (kT)^2 n_+ \tag{9}$$

$$Z = \frac{1}{n_e} \left[n_1 + 4n_2 + 9n_3 + \cdots \right]$$

$$q = \frac{kT}{e^2 Z n_+^{1/3}}$$

The numerical factor γ_E is tabulated in Ref. 7. The electron density n_e is calculated by use of the Saha equation.

Calculated values of Q_e are shown in Fig. 18. The electron–atom collision cross section is shown by broken
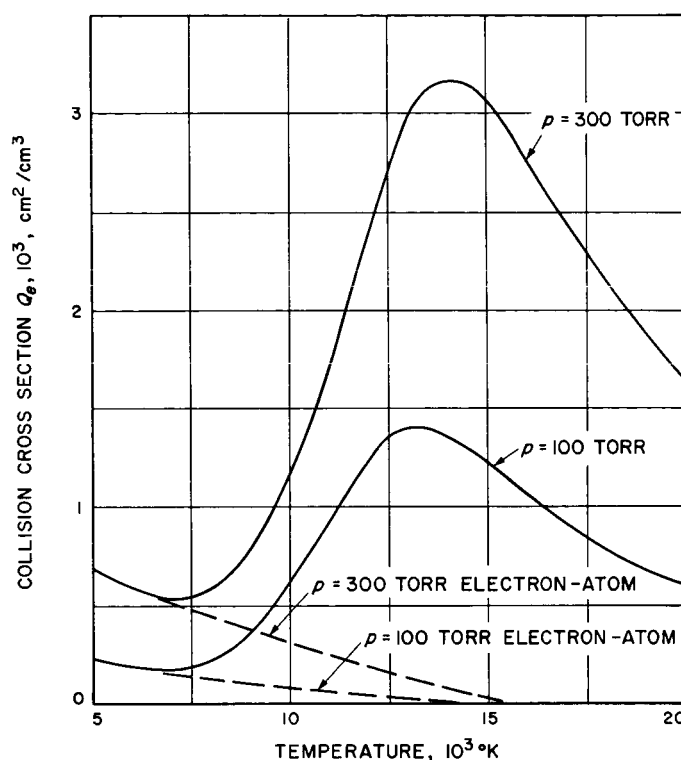

Fig. 18. Calculated electron collision cross section in argon

lines. It is seen that the cross section of collisions with ions becomes comparable to that of collisions with atoms at about 9,000°K. The total cross section has a maximum at around 13,000°K.

The electrical conductivity σ has been calculated by the expression given above. The results are shown in Fig. 19. Olsen's calculation for 1 atmospheric pressure (Ref. 5) is also shown. Below 11,000°K the conductivity does not depend on the pressure. At higher temperatures the conductivity is less for lower pressure. In the temperature range between 7,000°K and 12,000°K the conductivity varies almost linearly with the temperature and is approximated by

$$\sigma = s(T - T_c) \tag{10}$$

A thin straight line in the figure shows the approximate expression with $T_c = 7,000°K$ and $s = 1.2 \times 10^{-2}$ mho/deg cm. The approximate value is to be used in order to simplify the calculation of the heat balance.

The thermal conductivity of argon was calculated by Admur and Mason (Ref. 8) up to 15,000°K, ignoring the effect of ionization. When ionization takes place, the
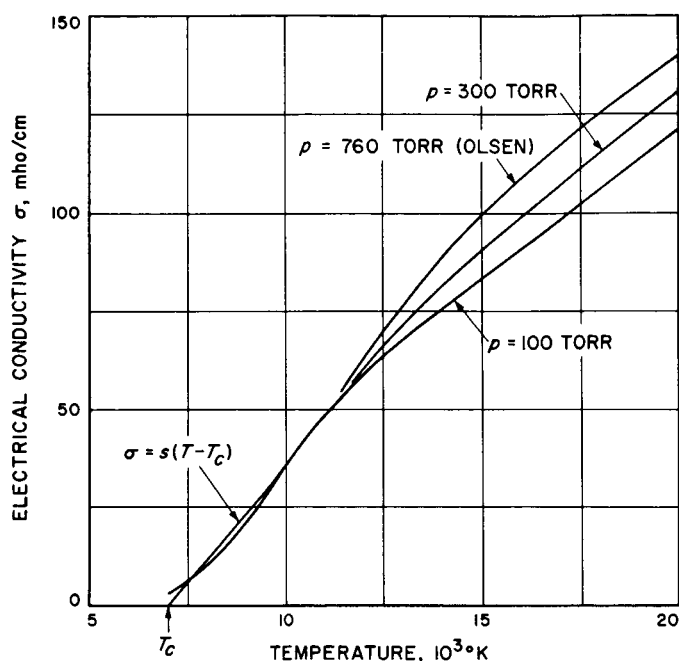
Fig. 19. Calculated electrical conductivity of argon

Fig. 20. Calculated thermal conductivity of argon
Pressure, 300 Torr

contribution of the electrons must be considered. According to Finkelnburg and Maecker (Ref. 9), the contribution is given by

$$K_e = \frac{1.25 \ n_e k \ \sqrt{3kT/m}}{Q_e} \qquad (11)$$

The total heat conductivity is expressed as

$$K = K_0 + K_e$$

Using Admur and Mason's value for K_0, K has been calculated for $p = 300$ Torr and is shown in Fig. 20. Spitzer and Härm (Ref. 7) give a formula for the fully ionized gas

$$K = 4.67 \times 10^{-12} \frac{T^{5/2}}{Z \log q} \delta_T \qquad (12)$$

This is shown in the figure by a chain line. The curve of partially ionized gas seems to be connected smoothly to that of fully ionized gas at high temperature. The thermal conductivity is approximated by

$$K = K_c \left[1 + \tau(T - T_c)^2\right] \qquad (13)$$

A thin line in Fig. 20 shows the approximate value for K with $T_c = 7,000°K$, $\tau = 3.8 \times 10^{-7}/deg^2$, $K_c = 6 \times 10^{-4}$ cal/sec deg cm. The approximate value is to be used for the heat balance calculation.

The enthalpy per unit volume is given by

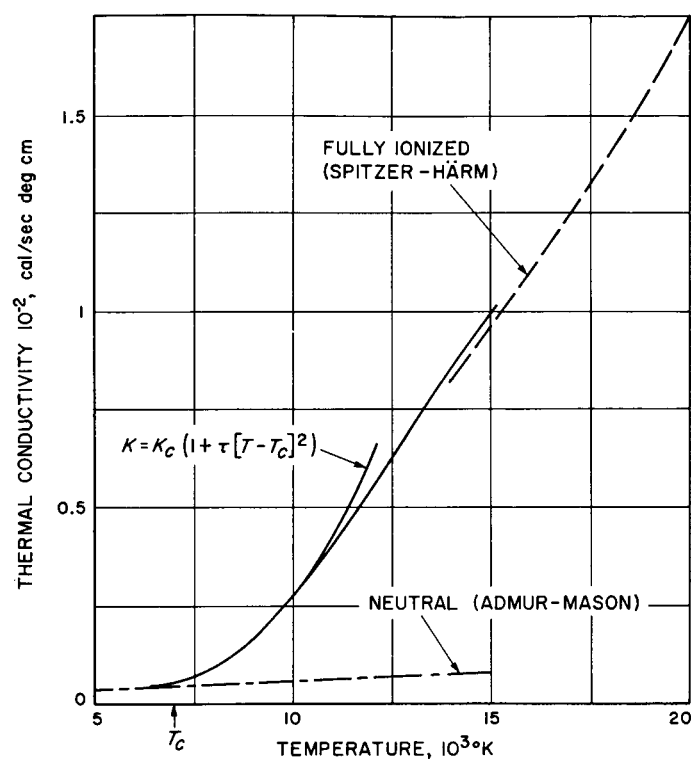$$H = \frac{5}{2} KTN + n_1 I_1 + n_2 (I_1 + I_2) \qquad (14)$$

where $N = n_0 + n_1 + n_2$, and I_1 and I_2 are the ionization potentials of the first and second ionization, respectively. Since the number density of each species is given by the Saha equation, H is easily calculated. The results are shown in Fig. 21. The enthalpy at 15,000°K is a factor of 3 greater than at low temperatures as a result of the ionization. For the heat balance calculation, H at $p = 300$ Torr is approximated by

$$H = 1 + 2.8 \left(\frac{T - T_c}{T_c}\right)^3 \qquad (15)$$

With $T_c = 7,000°K$, the approximate value is close to the exact value up to 12,000°K, as shown in Fig. 21.

When there is a temperature gradient in the plasma, there must be a number-density gradient, and the gradient causes diffusion. In plasma, the so-called ambipolar diffusion is predominant, and this is expressed as

$$energy \ flux = hD_i \frac{\partial n_i}{\partial x} = hD_i \frac{\partial n_i}{\partial T} \frac{\partial T}{\partial x}$$

in which h is the enthalpy per particle, and D_i is the diffusion coefficient. The factor $hD_i \cdot \frac{\partial n_i}{\partial T}$ is equivalent to the thermal conductivity. The diffusion coefficient D_i is
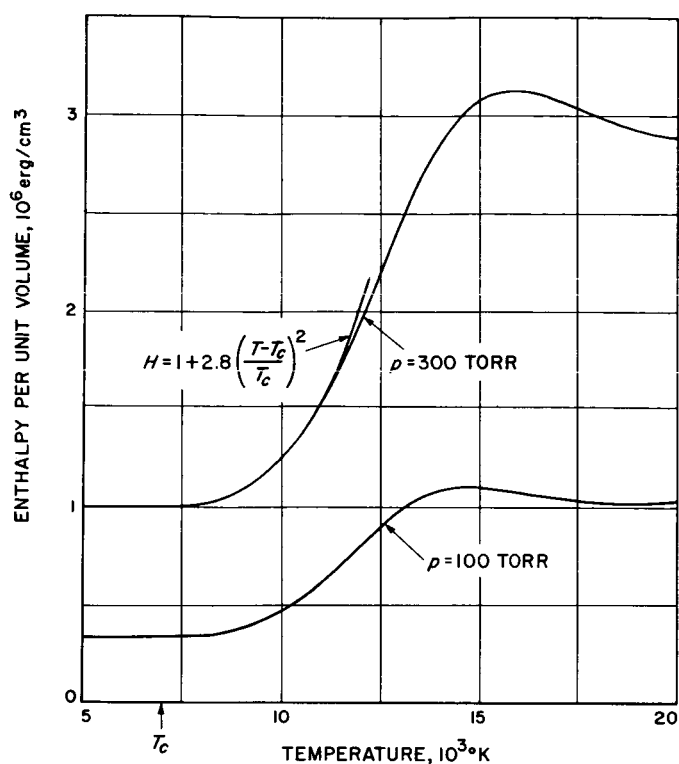
Fig. 21. Calculated enthalpy per unit volume of argon

estimated from existing data on ion mobility, and the Saha equation gives $\partial n_i/\partial T$. The calculation of the ambipolar diffusion indicates that the heat conduction is at least 10 times larger than the diffusion in the temperature range of present interest. The diffusion is therefore neglected in the heat balance calculation.

B. Heat Balance

The theoretical calculation of the heat balance in a positive column requires that some simplifications of the problem be made.

1. Ambipolar diffusion is neglected. The simple calculation described before shows that the effect of ambipolar diffusion on the energy flux is less than 10% of the heat conduction.

2. Radiation loss is neglected. No precise estimate of radiation is possible. However, a simple estimate shows that the radiation loss is much less than conduction.

3. Natural convection is neglected. Assuming the arc to be a horizontal solid cylinder, the convection velocity is estimated to be on the order of 1 meter/sec. As long as we are assuming the free-stream

velocity to be on the order of 10 meter/sec, the natural convection can be neglected.

4. Streamwise variations of the temperature distribution and flow field are not considered. This is a serious simplification. The variations of the temperature and flow in axial direction are small but not necessarily negligible. However, if the $\partial/\partial x$ term is retained, the fundamental equation becomes too complicated to be solved by present methods. Moreover, boundary conditions are not properly given at both ends of the plasma because our knowledge of the regions near the electrodes is not sufficient.

5. The flow field is assumed to be the same in the presence or absence of the arc. So far, there is no way of verifying this assumption because a flow measurement in the presence of an arc is almost impossible.

With these assumptions the heat balance is expressed as

$$\frac{1}{r}\frac{\partial}{\partial r}\left[r\left(VH - K\frac{\partial T}{\partial r}\right)\right] - \sigma E^2 = 0 \qquad (16)$$

In an integral form the balance of heat flux is given by

$$-2\pi r\, K\frac{\partial T}{\partial r} + 2\pi rVH - 2\pi E^2 \int_0^r \sigma\, rdr = 0 \qquad (17)$$

The three terms are conduction flux, convection flux, and Joule heat, respectively. The magnitude of each term is estimated as shown in Table 2 from the observed temperature distribution, electric field intensity, empirical formula for V (Eq. 5), and calculated values of K, σ, and H. The loss and gain are almost equal.

No simple analytical solution of Eq. (16) is expected, because K, σ, and H are complicated functions of temperature. The boundary condition on the center line is given by symmetry as

$$\partial T/\partial r = 0 \qquad \text{at } r = 0$$

Table 2. Heat balance per unit axial length, watt/cm (pressure, 300 Torr; free-stream velocity, 17 meter/sec; upstream cathode)

	Loss		Gain
	Conduction flux	Convection flux	Joule heat
$r = 0.33$ cm	42	8	35
$r = 0.54$ cm	67	13	76

A boundary condition at large r is, unfortunately, not given. Since the neglect of the streamwise variation is valid only for small r, boundary conditions cannot be given at $r = \infty$. Another objection to conditions at $r = \infty$ comes from the fact that E is not parallel to the arc axis at large r. Thus a meaningful solution of the equation might not extend to infinity. An alternative is to impose an artificial boundary condition, $T = T_c$ at $r = r_c$. For convenience, T_c is chosen as 7,000°K, at which the electrical conductivity is almost zero. For an arc burning in a free space, r_c is not given. Then, it is obvious from the fundamental equation that the parameters T_0, E, and r_c are not uniquely determined, but relations between them exist. Physically speaking, if we have an understanding of the processes occurring in the regions near the electrode, we might be able to determine T_0, E, and r_c.

Now T and r are nondimensionalized by

$$T - T_c = \theta \, T_c \text{ and } \eta = r/r_c$$

Then, a nondimensional fundamental equation is

$$\eta \theta'' \frac{K}{K_c} + \theta' \frac{K}{K_c} + \eta \frac{\partial K}{\partial T} \frac{T_c}{K_c} \theta'^2 + \eta \frac{r_c^2 \sigma}{K_c T_c} E^2$$

$$+ VH \frac{r_c}{K_c T_c} + \eta H \frac{r_c^2}{K_c T_c} \frac{\partial V}{\partial r} + \eta V \frac{r_c}{K_c} \frac{\partial H}{\partial T} = 0 \qquad (18)$$

in which prime indicates a differentiation with respect to η and K_c is the thermal conductivity at T_c. As shown before, σ, K, and H are approximated by

$$\sigma = sT_c\theta$$

$$K = K_c \left(1 + \tau T_c^2 \theta^2\right)$$

$$H = H_c \left(1 + \gamma \theta^3\right)$$

By proper choices of s, τ, and γ these expressions are good approximations to the calculated physical properties. The nondimensional differential equation becomes

$$\eta \theta'' \left(1 + \tau T_c^2 \theta^2\right) + \theta' \left(1 + \tau T_c^2 \theta^2\right) + 2\tau T_c^2 \theta \, \theta'^2 \eta$$

$$+ \eta \frac{r_c^2 s}{K_c} E^2 \theta + vh + \eta hv' + 3\eta v\gamma\theta^2\theta' = 0 \qquad (19)$$

in which $h = H/H_c$ and $v = V/U_1$.

Using Eq. (5), the nondimensional velocity distribution v is expressed as

$$v = -\frac{\delta}{\mu\eta} \left[\exp\left(-a\mu^2 \eta^2\right) - 1\right] \qquad (20)$$

in which $\mu = r_c/b$ and δ is a factor determined by the maximum value of v. Introducing nondimensional parameters α and β as

$$\alpha = \tau T_c^2$$

$$\beta = \frac{r_c^2 s}{K_c} E^2$$

the final expression of fundamental equation is given by

$$\eta \theta'' \left(1 + \alpha\theta^2\right) + \theta' \left(1 + \alpha\theta^2\right) + 2\alpha\eta\theta \, \theta'^2$$

$$+ \beta\eta\theta + vh + \eta hv' + 3\eta v \, \gamma \, \theta^2 \, \theta' = 0 \qquad (21)$$

A solution is obtained by a series expansion in η as

$$\theta = \theta_0 + C_2\eta^2 + C_4 \eta^4 + \cdots \qquad (22)$$

with boundary conditions

$$\theta' = 0 \qquad \text{at } \eta = 0$$

$$\theta = 0 \qquad \text{at } \eta = 1$$

The total current relation is given by

$$I = 2\pi E \int_0^{r_c} \sigma \, r dr$$

$$= 2\pi s T_c \, r_c^2 \, E \left(\frac{\theta_0}{2} + \frac{C_2}{4} + \frac{C_4}{6} + \frac{C_6}{8} \cdots\right) \qquad (23)$$

Numerical calculations were carried out for the case of $p = 300$ Torr, $U_1 = 17$ meter/sec, and $I = 70$ amp. At $p = 300$ Torr, the best values for s, τ, and γ are 1.2×10^{-2} mho/cm deg, $3.8 \times 10^{-7}/\text{deg}^2$, and 2.8, respectively. Terms of the series up to and including η^6 were considered. The results are shown in Fig. 22. Experimental values are also plotted. Agreement between the calculated and measured results is fairly good as far as the relationship between E and T_0 is concerned. The two radial distributions of temperature shown in Fig. 23 exhibit a disparity at large radius. There are two reasons to believe that the theoretical distribution might be the more correct one. One reason is based on a survey of the temperature around the arc made by use of a fine thermocouple. The thermocouple reading in this kind of measurement is very much affected by the radiation from the hot core of the arc, so that the observed temperature is usually higher than the true temperature. The survey showed much lower temperatures than an extrapolation of the spectroscopic result. Another reason
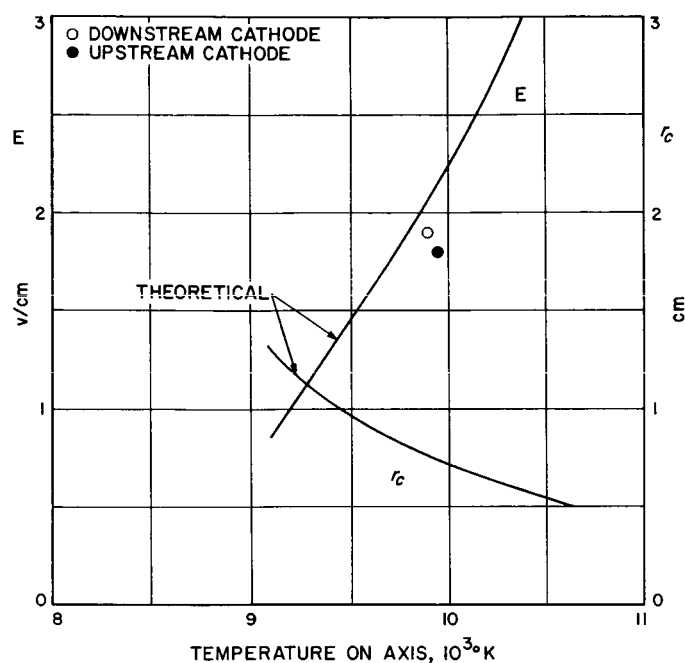
Fig. 22. Calculated electric field intensity and radius of long argon plasma column

Pressure, 300 Torr; free-stream velocity, 17 meter/sec

Fig. 23. Calculated temperature distribution

Pressure, 300 Torr; free-stream velocity, 17 meter/sec

is based on consideration of the stray light. As mentioned before, the light emitted by the low-temperature plasma is extremely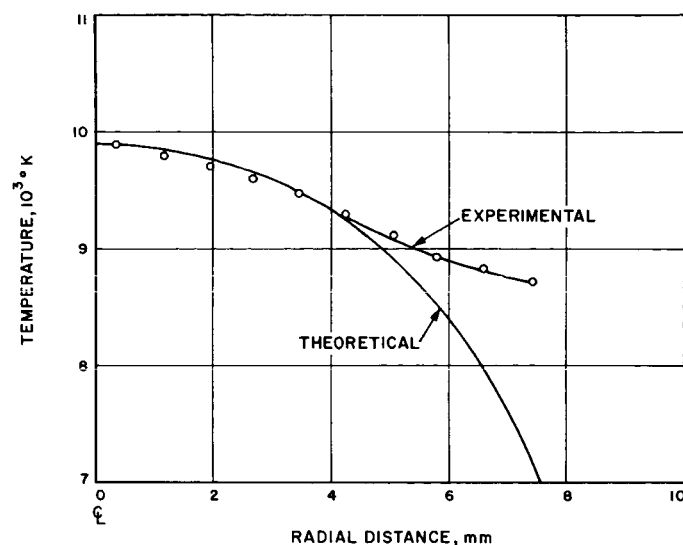 weak, and in the present method of measure-ment any stray light can be a source of error, with a tendency of making the apparent temperature higher.

In the foregoing calculation, however, the heat transfer due to the velocity fluctuation is not taken into account. It is well known that heat transfer and particle diffusion are enhanced by the presence of turbulence. A detailed investigation of this point is left to future efforts.

V. CONCLUSIONS

1. An arc discharge is stabilized by a flow parallel to the discharge. If the discharge current is kept constant, the electric field intensity of the positive column increases as the flow speed is increased. At a pressure of 300 Torr, the intensity at a free-stream velocity 27 meter/sec is twice that at zero velocity.

2. "Thermal pinch" was observed. In other words, the radius of the positive column decreases and the tempera-ture on the axis increases as the flow speed is increased.

3. When there is a flow around an arc, about one-quarter of the Joule heat generated in the positive col-umn is carried away by the radial forced convection and three-quarters by heat conduction.

4. The heat balance of the positive column was treated theoretically, neglecting an axial flow of heat. A relation between the temperature and electric field intensity was obtained. Theoretical and experimental results show a good agreement.

ACKNOWLEDGMENT

REFERENCES

1. Thiene, P. G., Chambers, J. E., and Jakowsky, W. V., *An Experimental Investigation of the Behavior of an Arc Positive Column in the Presence of Forced Convection,* Report 4 TN031-334, Plasmadyne Corp., Santa Ana, Calif., April 29, 1961.

2. Emmons, H. W., and Land, R. I., "Poiseuille Plasma Experiment," *Phys. Fluids,* Vol. 5, No. 12, 1962, pp. 1489–1500.

3. Sato, H., and Kuriki, K., "The Mechanism of Transition in the Wake of a Thin Flat Plate Placed Parallel to a Uniform Flow," *J. Fluid Mech.,* Vol. 11, Part 3, 1961, pp. 321–325.

4. Larenz, R. W., "Uber ein Verfahren zur Messung sehr hoher Temperaturen in nahezu durchlässigen Bogensäulen," *Z. Physik,* Bd. 129, 1951, pp. 327–342.

5. Olsen, H. N., "Thermal and Electrical Properties of an Argon Plasma," *Phys. Fluids,* Vol. 2, 1959, pp. 614–623.

6. Pearce, W. J., "Calculation of the Radial Distribution of Proton Emitters in Symmetric Sources," *Proceedings of the AFCRC Conference on Extremely High Temperatures,* H. Fischer and L. C. Mansur, Eds., John Wiley and Sons, New York, 1958.

7. Spitzer, L., Jr. and Härm, R., "Transport Phenomena in a Completely Ionized Gas," *Phys. Rev.,* Vol. 89, 1953, pp. 977–981.

8. Admur, I., and Mason, E. A., "Properties of Gases at Very High Temperatures," *Phys. Fluids,* Vol. 1, 1958, pp. 370–383.

9. Finkelnburg, W., and Maecker, H., *Handbuch der Physik,* Ch. XXII, "Gasentladungen," Springer-Verlag, Berlin, 1956.